We are IntechOpen, the world's leading publisher of Open Access books Built by scientists, for scientists

4,800
Open access books available

122,000
International authors and editors

135M
Downloads

Our authors are among the

154
Countries delivered to

TOP 1%
most cited scientists

12.2%
Contributors from top 500 universities

WEB OF SCIENCE™

Selection of our books indexed in the Book Citation Index in Web of Science™ Core Collection (BKCI)

Interested in publishing with us?
Contact book.department@intechopen.com

Numbers displayed above are based on latest data collected.
For more information visit www.intechopen.com

3

The Locally Adapted Scaling Vector Method: A New Tool for Quantifying Anisotropic Structures in Bone Images

Roberto Monetti et al.*
Max-Planck-Institut für extraterrestrische Physik, Garching
Germany

1. Introduction

Osteoporosis is a metabolic bone disorder in which bones become brittle and prone to fracture. According to the World Health Organization, it is characterized by the loss of bone mineral density and the deterioration of the bone micro-architecture (Prevention and Management of Osteoporosis, 2003). One of the most important factors in determining the risk of fracture is the bone strength. In clinical practice, the risk of fracture and the effects of drug therapy are assessed using only densitometric techniques as a quantitative measure (Kanis, 2002; Kanis, 2007).

Modern high-resolution imaging modalities like High-Resolution Computer Tomography (HRCT) and High-Resolution Magnetic Resonance Imaging (HRMRI) open up new possibilities to improve diagnostic techniques of osteoporosis since they are able to depict the architecture of trabecular bone. In particular, recent advances in MRI technology allow us to obtain images with in-plane spatial resolution as high as 50 μm in vitro and 150 μm in vivo, and a slice thickness of 128 μm in vitro and 280 μm in vivo (Link, et al., 1999; Carballido-Gamio et al., 2006; Wehrli, 2007; Krug et al., 2006). These figures should be compared with the actual thickness of the trabeculae, which ranges from 80 to 200 μm with an average size of approximately 120 μm. It has been shown that these imaging modalities enable the assessment of image data with respect to textural properties to detect structural differences (Boutry et al., 2003; Majumdar et al., 1996; Vieth et al., 2001).

HRCT is the preferred methodology to image bones. In contrast to MRI scans, CT scans can easily be calibrated using phantoms, thus rendering images with a standardize grey level distribution. In addition, CT images of the bone are free from the susceptibility artifacts and, in case of in vivo applications, have a less stringent requirement for patients to remain absolutely motionless during the scan as compared to MRI.

* Jan Bauer[2], Thomas Baum[2], Irina Sidorenko[1], Dirk Müller[2], Felix Eckstein[3], Thomas Link[4] and Christoph Räth[1]
[1]Max-Plack-Institut für extraterrestrische Physik, Garching, Germany, [2]Institut für Röntgendiagnostik, Technische Universität München, München, Germany, [3]Institute of Anatomy and Musculoskeletal Research, Paracelsus Private Medical University, Salzburg, Austria, [4]Magnetic Resonance Science Center, Department of Radiology, UCSF, San Francisco, CA, USA

Structure analysis techniques analogous to bone histomorphometry have been successfully applied in several in vivo studies of postmenopausal women to differentiate patients with and without osteoporotic fractures (Laib et al., 2002; Link et al., 2002; Majumdar et al, 1999; Phan et al., 2006; Link et al, 1998). However, these parameters, which are 2D linear measures, may show limitations when describing the complex 3D micro-architecture of human trabecular bone that contains non-linear correlations (Räth et al., 2003). It was shown in (Räth et al., 2003) that surrogate images generated from trabecular bone images which conserve the autocorrelation function display a different structure and can easily be distinguished using non-linear structure measures. On the other hand, texture measures extracted from HRMR and HRCT tomographic images of bone tissue using the Scaling Index Method (SIM) are well-suited for the description of the trabecular bone micro-architecture and its biomechanical properties (Baum et al., 2010; Müller et al., 2006). In contrast to the above mentioned 2D linear measures, bone structure parameters obtained using the SIM are 3D local texture measures which can account for the non-linear aspects of the trabecular network. The SIM is a tool inspired by the analysis of non-linear systems where it has been shown that global and local scaling properties of the phase space representation of a system provide useful information that characterize its underlying dynamics (Grassberger et al., 1998; Halsley et al., 1996; Paladini et al., 1987). This technique has also been successfully used in other fields of research, like astrophysics, biological applications and image processing (Räth et al., 2002; Räth et al., 2003; Jamitzky et al., 2000; Räth et al., 1997). Since the SIM considers different orientations on the image as equivalent, the derived structure parameters are isotropic. However, there are cases where the image structure reflects the anisotropy of the bone tissue. In fact, human proximal femur is a clear example where a large portion of bone tissue displays a mineralized trabecular network oriented along the major stress lines. The orientation of the trabecular structure is the result of the response of the mineral network growing mechanism to the external stimuli to maximize bone stability (Huiskes et al., 2000). Then, one expects that methods to predict bone mechanical properties based on image texture analysis will perform better when being able to quantify the intrinsic anisotropy of bone images.

Proximal femur fractures are the most severe complications of osteoporosis, with the highest morbidity and mortality (Center et al., 1999). Bone mineral density of the proximal femur measured using dual X-ray absorptiometry (DXA) is considered to be the standard technique for predicting fracture risk and the effects of drug therapy. DXA-based 2D-BMD is a bulk measure of mineralization that also accounts for the contribution of cortical bone, which is particularly important for the bone stability. Although BMD has already shown to have good correlation with bone strength, other properties of the bone like trabecular structure and connectivity may also contribute.

The aim of this chapter is to introduce a new methodology for the structure analysis of high-resolution tomographic images of human bone specimens able to account for orientations in the trabecular bone network. The so-called Locally Adapted Scaling Vector Method (LASVM) consists of two steps, namely the estimation of local main orientations and the subsequent application of an image structure analysis procedure that uses the previously obtained directional information. By means of the LASVM, we extract 3D non-linear texture measures, which locally take into account the anisotropic nature of the trabecular net. These measures are subsequently used to establish correlations with the biomechanical properties of bone specimens expressed via the fracture load. The purpose is to compare our results with those obtained using BMD, 2D morphometric parameters, and 3D isotropic texture

measures derived from the (isotropic) SIM. In addition, we investigate if multifactorial models utilizing BMD and structural parameters can predict bone strength better than BMD alone.

2. Material and methods

2.1 Femur specimens

Femur specimens were harvested from 148 formalin-fixed human cadavers. The donors had dedicated their body for educational and research purposes to the Institute of Anatomy in Munich prior to death, in compliance with local institutional and legislative requirements. Aside from osteoporosis, all pathological bone changes like bone metastases, hematological, or metabolic bone disorders were exclusion criteria for the study. Therefore, biopsies were taken from the iliac crest of all donors and examined histologically. Furthermore, radiographs were obtained from all specimens. If fractures, osteolytic changes, or other focal abnormalities were detected in the images, the respective donor was excluded from the study. Femur specimens that fractured during preparation or had distal shaft fractures in the biomechanical testing were also excluded. Using these criteria, 94 donors were included in the study, 55 females and 39 males. The donors had a mean age ± standard deviation (SD) of 80±10 years (range 52–100 years). The body height (BH) and body weight (BW) of each donor were measured. Surrounding soft tissue was completely removed from the femora and femoral head and neck diameter were measured. The head diameter was defined as the largest diameter of the femoral head in a plane orthogonal to the femoral neck axis. The neck diameter was the smallest diameter of the neck in a plane orthogonal to the femoral neck axis. For the purpose of conservation, all specimens were stored in formalin solution during the study. The specimens were degassed at least 24 hours before imaging to prevent air artifacts.

2.2 CT Imaging

CT images of the proximal femora were acquired for the structure analysis of the trabecular bone by using a 16-row Multislice Spiral CT scanner (Sensation 16; Siemens Medical Solutions, Erlangen, Germany). The specimens were placed in plastic bags filled with 4% formalin–water solution. The plastic bags were sealed after air was removed by a vacuum pump. These bags were positioned in the scanner with mild internal rotation of the femur to simulate the conditions as in an in vivo examination of the pelvis and proximal femur. Three specimens were scanned twice with repositioning to determine reproducibility. The applied scan protocol had a collimation and a table feed of 0.75 mm and a reconstruction index of 0.5 mm. Further scanning parameters were 120 kVp, 100 mA, an image matrix of 512 x 512 pixels, and a field of view of 100 mm. From a high-resolution reconstruction algorithm (kernel U70u) resulted an in-plane spatial resolution of 0.29 x 0.29 mm^2, determined at δ=10% of the modulation transfer function. Voxel size was 0.19 x 0.19 x 0.5 mm^3. For calibration purposes, a reference phantom with a bone-like and a water-like phase (Osteo Phantom, Siemens Medical Solutions) was placed in the scanner below the specimens.

2.3 CT Image processing

Three volumes of interest (VOIs) were fitted automatically in the trabecular part of the femoral head, neck, and greater trochanter. The algorithm was described in detail by Huber (Huber et al., 2008) for trabecular BMD analysis. The outer surface of the cortical shell of the

femur was segmented automatically by a threshold-based technique. The segmentation had to be corrected manually in 14 out of 94 cases due to thin cortical shell. Causes were focal bone loss due to advanced osteoporosis or adjacent anatomic structures, such as blood vessels, penetrating the cortex. After completed segmentation, an ellipsoid VOI was automatically fitted in the femoral head as well as a cylindric VOI in the femoral neck and an irregular VOI in the greater trochanter (Fig. 1). To obtain the head VOI, an ellipse was fitted to the superior bone surface points of the femoral head using a Gaussian– Newton least squares technique. The fitted ellipse was scaled down to 75% of its original size to account for cortical bone and shape irregularities of the femoral head and saved as head VOI. For the cylindrical neck VOI, an initial axis of the cylinder was established between the center of mass of the fitted ellipse and the intersection between the prolonged neck axis and the lateral bone surface. Based on this initial axis and the bone surface points of the neck, a first cube was fitted in the neck using a Gaussian–Newton least squares technique. The axis of the first cylinder was retained unchanged for the final cylinder. To account for cortical bone and shape irregularities, final cylinder length was defined as 65% of the radius of the first cylinder. The radius of the final cylinder was hereupon optimized by using the bone surface points of the neck. The final cylinder was saved as neck VOI. To define the trochanteric VOI, the cylinder axis was prolonged as far as the intersection with the lateral bone surface. Based on the relative position of the bone surface points to this intersection and the cylinder axis, surface regions corresponding to the trochanter, inferior part of the neck, and superior part of the shaft were determined. The surface region of the trochanter was used to fit a cone in the trochanter using a Gaussian–Newton least squares technique. The cone was discarded, but the relative position of the bone points to the fitted cone axis and the cylinder axis was assessed. According to their relative position, they were labeled as "trochanteric" or "nontrochanteric" bone points. The trochanteric bone points were saved as trochanteric VOI.

For all further image post-processing, images were interpolated to obtain isotropic datasets and reconstructed in a semi-coronal plane, oriented parallel to the axis of the femoral neck. For calibration purposes, a reference phantom (Osteo Phantom, Siemens) was placed below the specimens.

Fig. 1. Left: HRCT image of a human femur specimen with BMD = 0.69 g/cm^2 and FL = 3912 N (left). Middle: Binarized dataset according to the procedure explained in section 2.5. Right: Visualization of the fitted VOIs: head (ellipsoid), neck (cylinder), and trochanter (irregular) in the original CT data.

2.4 Biomechanical femoral bone strength

Absolute femoral bone strength was assessed with a biomechanical side-impact test measuring fracture load (*FL*), described in detail previously (Eckstein et al., 2004). In brief, a lateral fall on the greater trochanter was simulated. Femoral head and shaft were faced downward and could be moved independently from each other while the load was applied on the greater trochanter by using a universal testing machine (Zwick 1445; Zwick, Ulm, Germany) with a 10-kN force sensor and dedicated software. *FL* was defined as the peak of the load–deformation curve. Since *FL* depends on influencing variables such as bone size, relative femoral bone strength had to be appraised for better interpretation of the clinical utility. For appraisal of the relative bone strength, *FL* was adjusted femoral neck length (*FNL*). For this purpose, *FL* was divided by this parameter.

2.5 Morphometric parameters

In a first step, it was defined, which pixels should be interpreted as bone ("on"-pixels), and which as marrow ("off"-pixels). The binarization of the CT images was required to evaluate the 2D morphometric parameters. We applied an optimized global threshold to all images. To optimize this threshold, we evaluated thirty characteristic proximal femur images visually, and determined the best threshold to be 200 *g/cm³* hydroxyapatite. This hydroxyapatite threshold (Λ_{Ca}) was converted to Hounsfield units (HU) for every image using the following expression

$$\Lambda_{\mathrm{HU}} = \frac{(B_{\mathrm{HU}} - W_{\mathrm{HU}})}{(B_{Ca} - W_{Ca})}\Lambda_{Ca} + W_{\mathrm{HU}}\,, \tag{1}$$

where Λ_{HU} is the grey level threshold in HU, Λ_{Ca} is the threshold evaluated in *g/cm³* of hydroxyapatite, B_{Ca} is the bone-like phase of the reference phantom in *g/cm³* of hydroxyapatite, B_{HU} is the bone-like phase of the reference phantom in HU, W_{Ca} is the water-like phase of the reference phantom in *g/cm³* of hydroxyapatite, and W_{HU} is the water-like phase of the reference phantom in HU. For further details see (Bauer et al., 2006).

After binarization, four morphometric parameters were calculated in analogy to standard histomorphometry using the mean intercept length method (Parfitt et al., 1987): bone fraction (BF) (resulting from bone volume divided by total volume), trabecular number (TbN), trabecular spacing (TbSp), and trabecular thickness (TbTh). It should be noted that the values of these parameters are considered as apparent values, since, given the limited spatial resolution, they cannot depict the true trabecular structure.

2.6 Local anisotropic structure analysis

A simple visual inspection of images of trabecular bone tissue reveals that the trabecular network and marrow bone areas are not evenly distributed. In addition, the trabecular structure of some human bones is essentially anisotropic, i.e. clear preferential directions of the mineral network are observed as a result of its growing mechanism. These image features suggest that a suitable method to assess the bone structure must be able to quantify local structure differences and account for the anisotropy of the mineral network. We propose a methodology which consists of two steps, namely the estimation of local main orientations and the subsequent application of a local image structure analysis procedure which uses the previously obtained directional information. This method, which is a variant of the Scaling Index Method (Böhm et al., 2003; Monetti et al., 2003; Müller et al., 2006),

differs from previous approaches where only an average global directionality on images was considered (Monetti et al., 2004). Recently, the SIM has been applied to μ-CT images of trabecular bone (Monetti et al., 2007; Räth et al., 2008; Monetti et al., 2009) where it was demonstrated that the use of directional information allows identifying the most important load-bearing bone substructures.

As shown below, any suitable method to estimate directions in 2D or 3D can be coupled to this structure characterization procedure. Several methods have already been developed to measure the trabecular bone orientation like the tensor scale algorithm (Saha et al., 2004) or methods based on image skeletonization (Saha et al., 2000; Gomberg et al., 2000; Wehrli et al., 2001). Here, we will restrict ourselves to local directions on the image plane and estimate them using a local directional filter. For the sake of clarity, we first describe the image structure characterization procedure. Then, it becomes evident how the orientations can be coupled to it.

The SIM is a procedure to extract information from multidimensional, arbitrary point distributions by assessing local pointwise dimensions, i.e. the scaling indices, for each data point. Consider a 3*D* tomographic image where a gray value *g* = *G(x, y, z)* is assigned to each pixel. Thus, each pixel contains space and gray value information that can be encompassed in a four dimensional vector $\vec{p} = \left[x, y, z, G(x, y, z) \right]$. Then, the 3*D* tomographic image *G(x, y, z)* has been mapped onto a 4*D* point distribution which contains both the spatial and grey level information. For each point in the phase space, the number *N* of points located within an 4-dimensional sphere of radius *L* centered at $\vec{p}_i$ is counted,

$$N(\vec{p}_i, L) = \sum_j \Theta\left(L - \left\| \vec{p}_j - \vec{p}_i \right\| \right), \tag{2}$$

where $\Theta(x) = 1$ if $x \geq 0$ and $\Theta(x) = 0$ otherwise, is the Heaviside function. The distribution $N(\vec{p}_i, L)$ is evaluated within the so-called scaling range $L \in [L_1, L_2]$. In most of the cases, one finds that $N(\vec{p}_i, L)$ behaves approximately as a power-law when increasing *L*, i.e. $N(\vec{p}_i, L) \propto L^{\alpha_i}$. The scaling-index α_i can be estimated by the difference ratio

$$\alpha_i = \left[\log\left(N(\vec{p}_i, L_2) \right) - \log\left(N(\vec{p}_i, L_1) \right) \right] / \left[\log(L_2) - \log(L_1) \right], \tag{3}$$

where L_1 and L_2 are specified by the lower and upper limit of the scaling range. This scalar quantity contains information of the underlying local structure around $\vec{p}_i$. For instance, given a 3*D* point distribution, different structural elements like rods, plates, and a random background will lead to scaling index values $\alpha \approx 1$, $\alpha \approx 2$, $\alpha \approx 3$, respectively (Müller et al., 2006). The assessment of cancellous bone local structure type is an important issue already investigated using the so-called structure model index (SMI) (Hildebrand et al., 1997). This technique also allows the quantification of plate, rod objects or mixture of plates and rods by using an index value. The SMI was defined as a value between 0 and 3. For an ideal plate structure the structure model index value is 0 and it is 3 for an ideal rod structure. For a structure with both plates and rods of equal thickness, the value is between 0 and 3, depending on the volume ratio between rods and plates. The calculation of the SMI requires a binarization of the images. Typical applications of the SMI are connected to the use of μ-CT images. These studies (Hildebrand et al., 1999; Ding et al., 2000) address questions like

age-related cancellous bone structure changes and demonstrate the cancellous bone structure variability for different skeletal sites.

Scaling indices can also be calculated using a different method. In general, instead of calculating $N(\vec{p}_i, L)$, it is possible to define a local weighted cumulative point distribution ρ as

$$\rho(\vec{p}_i, R) = \sum_j \exp\left(-\left(d(\vec{p}_i, \vec{p}_j) \Big/ R\right)^q\right), \tag{4}$$

where R is the scale parameter and $d(\vec{p}_i, \vec{p}_j)$ a distance measure. The exponent q controls the weighting of points according to their distance to the point where the scaling index is calculated. For small values of q, points in a broad region around $\vec{p}_i$ significantly contribute to the weighted local density $\rho(\vec{p}_i, R)$. As q increases, the shaping function becomes more and more step-like counting all points with $d(\vec{p}_i, \vec{p}_j) < R$ and neglecting all points with $d(\vec{p}_i, \vec{p}_j) > R$. Here, we use q=2. The scaling index α_i is defined as the logarithmic derivative of ρ with respect to R, $\alpha = \frac{\partial \ln \rho}{\partial \ln R}$. Thus one obtains

$$\alpha_i = \frac{\sum_j 2\left(\frac{d(\vec{p}_i, \vec{p}_j)}{R}\right)^2 \exp\left(-\left(\frac{d(\vec{p}_i, \vec{p}_j)}{R}\right)^2\right)}{\sum_j \exp\left(-\left(\frac{d(\vec{p}_i, \vec{p}_j)}{R}\right)^2\right)}. \tag{5}$$

Using this procedure, scaling indices are expressed analytically and depend only on the parameter R. We call them weighted scaling indices.

Let us now focus on the distance measure $d(\vec{p}_i, \vec{p}_j)$. A generalized quadratic distance measure can be written as follows

$$d^2\left(\Delta\vec{p}_{ij}\right) = \Delta\vec{p}_{ij}{}^T A \Delta\vec{p}_{ij}, \tag{6}$$

where $A = U^T W U$ is a non-singular matrix, U is the rotation matrix and W is a diagonal matrix containing the eigenvalues of the matrix A. As in (Müller et al., 2006), the tomographic image $g = G(x, y, z)$ is mapped onto a 4D space as $\vec{p}(x, y, z, g) = (x, y, z, G(x, y, z))$. Thus, a 4D rotation matrix has to be used. The only meaningful rotations are rotations in the spatial 3D space. We consider rotations on the image plane, i.e. rotations around the z-axis. The reason for this choice is that we are using CT images of sagittal sections of the femur. We assumed no large directional changes outside the image plane (z=constant), since the mineralized trabeculae are mostly oriented along the major stress lines. The rotation matrix reduces to

$$U = \begin{pmatrix} \cos\theta & -\sin\theta & 0 & 0 \\ \sin\theta & \cos\theta & 0 & 0 \\ 0 & 0 & 1 & 0 \\ 0 & 0 & 0 & 1 \end{pmatrix}, \tag{7}$$

where θ is the rotation angle around the *z*-axis. The quadratic distance measure can be written as

$$d^2\left(\Delta\vec{p}_{ij}\right) = \lambda_x\left(\Delta x_{ij}\cos\theta + \Delta y_{ij}\sin\theta\right)^2 + \lambda_y\left(\Delta x_{ij}\sin\theta - \Delta y_{ij}\cos\theta\right)^2 + \lambda_z\left(\Delta z_{ij}\right)^2 + \lambda_g\left(\Delta g_{ij}\right)^2, \tag{8}$$

where the eigenvalues $\lambda_{k=\{x,y,z,g\}}$ are the weighting factors of the three orthogonal spatial directions and the grey-level axis, respectively. When all directions have the same weight, i.e. $\lambda_x = \lambda_y = \lambda_z = \lambda_g$, we obtain $A=I$, and d^2 becomes the (isotropic) Euclidean distance. We observe that the choice of different λ values allows us to assign different weights for the directions. It becomes clear from Eq. (8) that this variant of the SIM allows for the input of local orientations. For points where no clear directionality is observed it is always possible to set $\lambda_x = \lambda_y = \lambda_z$.

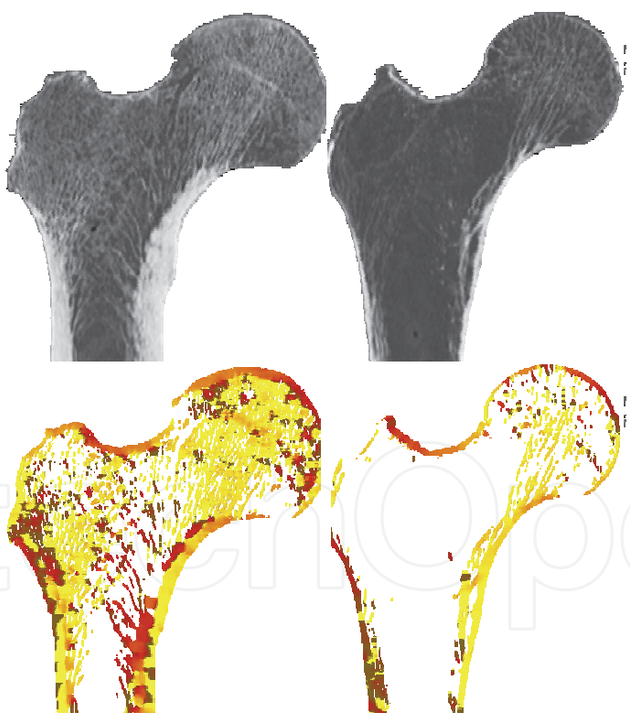

Fig. 2. First row: HRCT images of a healthy and an osteoporotic specimen. Second row: Color-represented orientation map. Trabeculae displaying the same directionality are coded with the same color. The orientations are calculated at every pixel for every bone slice.

Eq. (8) also indicates that the parameter λ_z can be used to account for the different in plane and normal to the plane resolutions and λ_g as a normalization factor for the grey level distribution. Because of the flexibility that this variant of the SIM offers, we call it the

"Locally Adapted Scaling Vector Method" (LASVM). It should be noted that the LASVM reduces to the original isotropic SIM when we set $\lambda_x = \lambda_y = \lambda_z$ for all points of the distribution. In the following, we will simply call scaling indices to the indices calculated using the "isotropic" SIM. Scaling indices obtained with LASVM are called "scaling vectors".

2.7 Calculation of the bone orientation map

To calculate local orientations of the trabecular network, we consider the CT images binarized according to the procedure given in section 2.5 (see Fig. 1 central panel). Then, the binarized images (2D CT slices) were skeletonized using the classical thinning algorithm. The predominant orientation Θ was calculated for every pixel having two neighbour pixels (defined as "rod-like" pixel), thus connection points or end points of the skeleton were excluded. To determine the final orientation map, every "bone" pixel of the binarized image was assigned the value of the orientation of the nearest rod-like pixel of the skeleton. The degree of anisotropy at every pixel was defined as $1/\sigma(\Theta)$, where $\sigma(\Theta)$ is the standard deviation of the orientations within a surrounding neighborhood of 7x7 pixels. Here, all orientations at "bone" pixels having a degree of anisotropy larger than 2 were considered. Image pixels that do not carry directional information were treated as isotropic, thus $\lambda_x = \lambda_y = \lambda_z$. Figure 2 shows typical examples of orientation maps for two femur specimens that have different bone mineral density. The colors indicate the angles evaluated using the procedure described above. It should be emphasized that the image structure characterization procedure is neither restricted to the use of orientations in 2D nor to the particular method to evaluate local directions. In fact, any suitable method to determine orientations can be coupled to the LASVM.

2.8 The structure measures

In order to quantify bone structural differences among specimens, the local information given by the scaling indices or scaling vectors is compiled in the so-called $P(\alpha) = \Pr(\alpha \in [\alpha, \alpha + d\alpha])$ probability density of scaling vectors or $P(\alpha)$ spectrum. As an example, we consider two dimensional binary toy images containing line-like elements and a noisy background (see Fig. 3). The purpose is to demonstrate how the sensitivity to the underlying anisotropy is enhanced, when using an anisotropic distance measure. Both images have exactly the same number of line-like elements and background points. The top-left image in Fig. 3 displays a pattern with no clear main directionality while the top right one shows a main direction given by an angle $\beta = 45^\circ$ measured from the horizontal in the clockwise direction.

The bottom-left spectra shown in Fig. 3 were calculated applying the SIM to the upper images, i.e. using an isotropic distance measure. We observe that both spectra are quite similar, thus the clear anisotropy of the top right image is not accounted by the SIM. However, the bottom-right spectra (see Fig. 3) indicate that the use of an anisotropic distance measure enhances the contrast between the spectra and thus the sensitivity to the underlying anisotropy of the image.

Fig. 4 (upper row) shows $P(\alpha)$ spectra obtained using the (isotropic) SIM for the three segmented VOI's, i.e. femur head, neck and trochanter. We observe structural differences at the femur neck and trochanter, while the $P(\alpha)$ spectra from the femur head are quite similar.

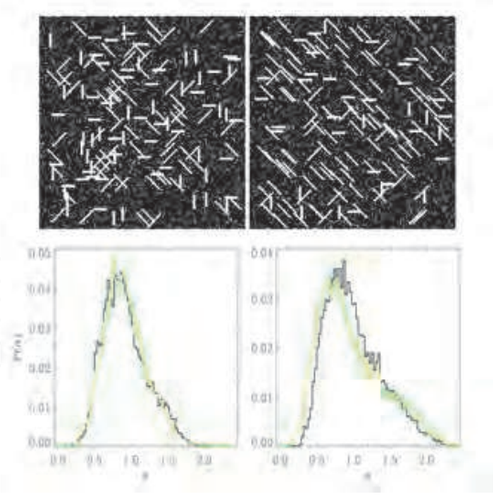

Fig. 3. Upper left: 2D toy image where a random background has been combined with randomly oriented lines. Upper right: 2D toy image where a random background has been combined with lines displaying a specific global orientation of β = 45° with respect to the horizontal measured in the clockwise direction. The number of lines and background points is the same in both images. Lower left: $P(\alpha)$ spectra of the toy images obtained using the isotropic SIM. Lower right: $P(\alpha)$ spectra of the toy images obtained using the LASVM in 2D. Black curves are the spectra of the upper left image and green curves are the ones for the upper right image.

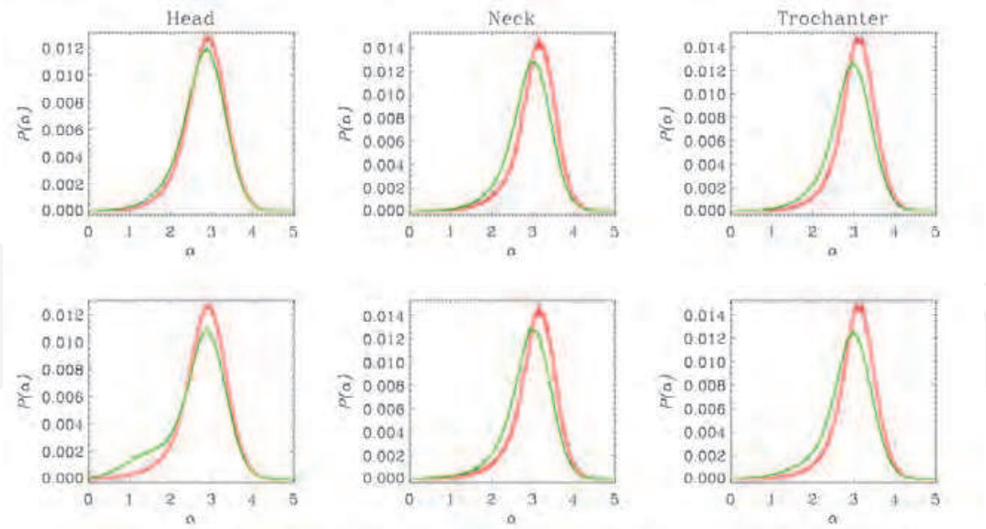

Fig. 4. $P(\alpha)$ spectra for the different VOI's of the proximal femur specimens. The green (red curve) spectrum corresponds to a specimen with BMD_DXA = 0.69 *g /cm²* and *FL* = 3910 N (BMD_DXA = 0.69 *g /cm²* and *FL* of 2450 N), respectively. From left to right, the plots show $P(\alpha)$ of the femur head, neck, and trochanter, respectively. Upper row: $P(\alpha)$ spectra obtained using an isotropic distance measure. Lower row: $P(\alpha)$ spectra for the same VOI's obtained using an anisotropic distance measure.

Figure 4 (lower row) shows the $P(\alpha)$ spectra calculated using the (anisotropic) LASVM. Now, the largest structural difference is observed in the femur head. These differences are the result of this novel structural characterization that takes into account the bone orientation map. Spectra corresponding to the femoral neck and trochanter are very similar to those calculated using the isotropic distance measure. This situation occurs in the absence of strongly oriented trabecula within the VOI, thus scaling vectors reduce to (isotropic) scaling indices. Then, we conclude that directionality assessment considerably enhances the contrast between $P(\alpha)$ spectra (see Fig 4, lower left) and improves the bone structure characterization procedure. This result is in agreement with that obtained from the analysis of the toy images.

Fig. 5 shows two HRCT image slices for specimens with equal BMD_DXA values but very different *FL* values. The color-coded femur sections are the corresponding α-images, i.e. the

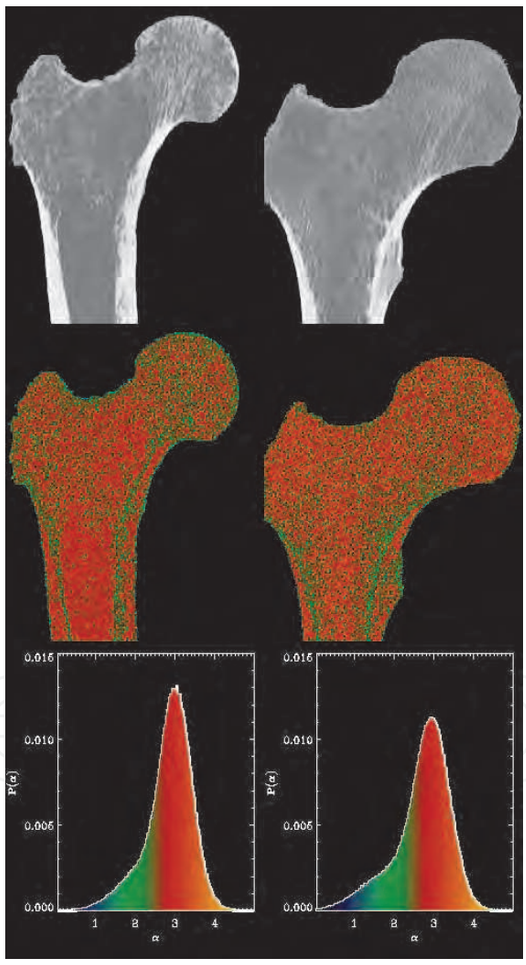

Fig. 5. First Row: HRCT images of two femur specimens with the same BMD_DXA = 0.83 and different *FL* = 2939 *N* (left) and *FL* = 6717 *N*. Second Row: Color-coded α-images of the specimens shown in the first row. Third Row: Color-coded $P(\alpha)$ spectra which helps identifying the local structures on the α-images. These results were obtained using scaling vectors.

images created using the values of the scaling vectors. Panels in the lower row of Fig. 5 show the color-coded $P(\alpha)$ spectra for the two femur specimens where the same color-coding as for the α-images was used. It is then clear that the trabecular bone structure mainly corresponds to the green-dark yellow region of the α-images, i.e. $1 < \alpha < 2.7$. We observe that the $P(\alpha)$ spectrum of the weaker femur specimen is shifted to higher α–values, thus reflecting a higher frequency of structureless (homogeneous) regions. However, the stronger femur specimen has a larger contribution of α–values corresponding to trabecular structure.

We perform a correlation analysis based on a filtering procedure applied to the $P(\alpha)$ spectrum, which considers one sliding window of variable width. Filtering procedures based on sliding windows have successfully been applied for the characterization of the bone micro-architecture in other studies (Böhm et al., 2003; Monetti et al., 2003). A characteristic quantity, called the α–fraction $\Delta_w P(\alpha)$, is extracted from the $P(\alpha)$ spectrum. Let α_i, and w be the position and width of the sliding window, respectively. We call α-fraction, the fraction of pixels with scaling vector values within the sliding window $[\alpha_i, \alpha_i + w]$. Thus, the α–fraction $\Delta_w P(\alpha)$ accounts for the structural content in window w. It should be noted that one has a simple scalar value $\Delta_w P(\alpha)$ for each individual specimen. The position and width of the window has been chosen to achieve optimal correlation between $\Delta_w P(\alpha)$ and FL. It should be noted that this kind of correlation analysis may lead to high correlation coefficients that must be disregarded. In order to avoid these outliers, one has to check if correlation coefficients are stable over a neighborhood of window positions and widths around the optimal value. Second, since our methodology allows us to retrieve the image pixels from the $P(\alpha)$ spectra, one has to check if the selected volume belongs to a particular bone substructure or corresponds to structureless marrow bone regions. It should be mentioned that our sample was not split into training and test samples due to its small size, which is otherwise the standard procedure to follow. All our results were obtained using $\lambda_g = (60/\sigma_g)^2$ and $R = 2.5$, where σ_g is the standard deviation of the grey level distribution in the VOI. We have chosen $\lambda_x = 50\lambda_y = 50\lambda_z$ to account for the local anisotropy of the trabecular structure. This defines an ellipse on the image plane of major axis approximately 14 pixels and a minor axis of 3. This eccentricity was suitable to account for anisotropy within a typical scale of the size of the apparent mean trabecular width. It should be noted that the value $\lambda_g = (60/\sigma_g)^2$ normalizes the standard deviation of the grey level distribution of the images to $\sigma_g = 60$. This is a suitable normalization choice that allows us to compare the spatial scales with the grey level scale and thus computing the distance in the above defined 4D space.

3. Results and discussion

Relationships among FL, $\Delta_w P(\alpha)$, BMD, and the 2D morphometric parameters were obtained using a linear regression analysis and a two-tailed t-test of significance as well. We have also studied the relationship between FL and the combination of a bone structure measure and BMD using a multivariate regression analysis. For the multiregression analysis, we have considered linear combinations of a structure measure and both the bone mineral density evaluated for the whole femur using DXA (BMD_DXA) and the bone

mineral density evaluated for the individual VOI using QCT (BMD_QCT). In all cases, Spearman's correlation coefficients were calculated. We obtain a correlation *r=0.73* for *FL* versus BMD_DXA of the whole femur. All other results are summarized in Tables 1 to 5. Table 1 shows the correlation coefficients of both the morphometric parameters and BMD_QCT versus *FL* for the different VOI. Tb.Sp is the morphometric parameter that correlates best with *FL*, when evaluated in the femur head (r_H = 0.72). All morphometric parameters evaluated in the femur head and neck lead to moderate correlations, while those calculated in the femur trochanter lead to lower correlation coefficients. Table 2 shows that for models combining the morphometric parameters and BMD_DXA, the prediction of femur mechanical properties is greatly improved. The best result is obtained for the femur head. However, Table 2 also indicates that BMD_QCT provides no additional information for the prediction of biomechanical strength, since some of the correlation coefficients become lower than those obtained using the morphometric parameters alone.

FL versus	BF	Tb.N	Tb.Sp	Tb.Th	BMD_QCT
r_H	0.64	0.31	-0.72	0.46	0.58
r_N	0.61	0.61	-0.51	0.58	0.58
r_{Tr}	0.49	0.52	-0.53	0.31	0.49

Table 1. Correlation coefficients calculated for the different VOI, i.e. femur head (r_H), neck (r_N), and trochanter (r_{Tr}), of the morphometric parameters versus the fracture load. The correlation coefficients of the bone mineral density evaluated using QCT versus *FL* are also shown.

FL versus	Tb.N	Tb.Sp	Tb.Th
r_H^D	0.78	0.76	0.76
r_N^D	0.76	0.76	0.76
r_{Tr}^D	0.76	0.76	0.76
r_H^Q	0.55	0.56	0.46
r_N^Q	0.54	0.55	0.55
r_{Tr}^Q	0.51	0.54	0.52

Table 2. Correlation coefficients indicated with a superscript "D" were calculated for the different VOI's using a linear multiregression model combining morphometric parameters and BMD_DXA. The coefficients indicated with a superscript "Q" were evaluated for the different VOI's using a linear multiregression model combining the morphometric parameters and the BMD_QCT of the respective VOI.

The results obtained using scaling indices are summarized in Tables 3-8. Table 3 shows that the α–fraction leads to low correlation coefficients versus *FL* for the three VOI's. For the femur head and femur neck, the bone structure that lead to the best correlations corresponds to trabecular structure. However, for the femoral trochanter, the α–fraction corresponds to marrow bone regions.

FL versus	*r*	Δ_w
$\Delta_w P_H(\alpha)$	0.42	$\alpha \in [2.09, 3.46]$
$\Delta_w P_N(\alpha)$	0.40	$\alpha \in [2.72, 2.86]$
$\Delta_w P_{Tr}(\alpha)$	0.13	$\alpha \in [4.43, 4.54]^*$

Table 3. Correlation coefficients for the α-fraction $\Delta_w P(\alpha)$ versus *FL* for the different VOI. The $P(\alpha)$ spectra were evaluated using an isotropic distance measure. The intervals show the region of the spectrum leading to the highest correlation coefficient. (*) Interval corresponding to marrow bone regions.

Table 4 shows results of a multiregression analysis combining the α–fraction and BMD_DXA for the three VOI's. We observe that the use of structural information lead to correlation coefficients higher than that obtained using BMD_DXA alone (r=0.73). However, only the α–fraction of the femoral head corresponds to the trabecular bone structure. Table 5 shows results of a multiregression analysis where the α–fraction has been combined with the BMD_QCT of the corresponding VOI's. We observe that correlations do not increase, thus the structural information is redundant in this case.

FL versus	r^D	Δ_w
$\Delta_w P_H(\alpha)$	0.79	$\alpha \in [2.03, 3.49]$
$\Delta_w P_N(\alpha)$	0.78	$\alpha \in [4.28, 4.42]^*$
$\Delta_w P_{Tr}(\alpha)$	0.78	$\alpha \in [3.68, 3.88]^*$

Table 4. Correlation coefficients calculated for the different VOI obtained using a linear multiregression model combining the α-fraction $\Delta_w P(\alpha)$ and BMD_DXA. The $P(\alpha)$ spectra were evaluated using an isotropic distance measure. (*) Interval corresponding to marrow bone region.

FL versus	*r*	Δ_w
$\Delta_w P_H(\alpha)$	0.52	$\alpha \in [2.12, 3.46]$
$\Delta_w P_N(\alpha)$	0.54	$\alpha \in [4.31, 4.51]^*$
$\Delta_w P_{Tr}(\alpha)$	0.56	$\alpha \in [3.62, 3.88]^*$

Table 5. Correlation coefficients calculated for the different VOI obtained using a linear multiregression model combining the α-fraction $\Delta_w P(\alpha)$ and BMD_QCT evaluated within the respective VOI. The $P(\alpha)$ spectra were evaluated using an isotropic distance measure. (*) Interval corresponding to marrow bone region.

Table 6 shows correlation results of *FL* versus the α-fraction extracted from $P(\alpha)$ spectra evaluated with the LASVM. We observe that the correlation coefficient for the femur head is significantly higher than that obtained using scaling indices (r_H=0.42). Even though moderate correlations are obtained at the femoral neck, the bone substructure leading to the highest correlation coefficient is the trabecular network. The femoral trochanter leads to a low correlation coefficient for an α–fraction corresponding to marrow bone regions. Note,

however that this result is not significant. A multiregression analysis combining the α–fraction of the femoral head and BMD_DXA (see Table 7) leads to the highest correlation coefficient obtained in this analysis (r_H^D=*0.80*). Results for the multiregression model calculated for other VOI's are considered not significant.

FL versus	*R*	Δ_w
$\Delta_w P_H(\alpha)$	0.66	$\alpha \in [2.39, 3.21]$
$\Delta_w P_N(\alpha)$	0.37	$\alpha \in [2.72, 2.86]$
$\Delta_w P_{Tr}(\alpha)$	0.17	$\alpha \in [4.46, 4.54]^*$

Table 6. Correlation coefficients of the α-fraction $\Delta_w P(\alpha)$ versus *FL* for the different VOI. The $P(\alpha)$ spectra were evaluated using an anisotropic distance measure. The intervals show the region of the spectrum leading to the highest correlation coefficient. (*) Interval corresponding to marrow bone region.

FL versus	r^D	Δ_w
$\Delta_w P_H(\alpha)$	0.80	$\alpha \in [2.57, 3.07]$
$\Delta_w P_N(\alpha)$	0.78	$\alpha \in [4.28, 4.51]^*$
$\Delta_w P_{Tr}(\alpha)$	0.78	$\alpha \in [3.68, 3.94]^*$

Table 7. Correlation coefficients calculated for the different VOI obtained using a linear multiregression model combining the α-fraction $\Delta_w P(\alpha)$ and BMD_DXA. The $P(\alpha)$ spectra were evaluated using an anisotropic distance measure. (*) Interval corresponding to marrow bone region.

FL versus	r^Q	Δ_w
$\Delta_w P_H(\alpha)$	0.66	$\alpha \in [2.36, 3.25]$
$\Delta_w P_N(\alpha)$	0.54	$\alpha \in [4.31, 4.51]^*$
$\Delta_w P_{Tr}(\alpha)$	0.56	$\alpha \in [3.68, 3.88]^*$

Table 8. Correlation coefficients calculated for the different VOI obtained using a linear multiregression model combining the α-fraction $\Delta_w P(\alpha)$ and BMD_QCT evaluated within the respective VOI. The $P(\alpha)$ spectra were evaluated using an anisotropic distance measure. (*) Interval corresponding to marrow bone region.

Finally, Table 8 shows results of a multiregression analysis where the α–fraction has been combined with the BMD_QCT of the correspoding VOI's. We observe that the correlations do not increase, thus the information provided by the combined quantities is redundant.
In summary, the structure measure obtained using the LASVM leads to a correlation coefficient *r=0.66* versus *FL* for the femoral head. This value is comparable to that given by BMD_DXA (*r*=0.73) and the best histomorphometric parameter Tb.Sp (*r*=0.72). It should be mentioned that our analysis was performed on VOI's which were defined automatically by means of geometrical considerations only. Since most of the fractures in the mechanical test

occurred in the femoral neck, better correlations with *FL* might be obtained when using a larger VOI, including the whole femur neck and the distal part of the femur head. Considering that the α-fraction is a simple measure of structure, a better prediction of the biomechanical properties of the human femur is also expected when applying more refined quantities extracted from the bone structural characterization given by the LASVM.

A linear multiregression model combining the α-fraction calculated at the femoral head using the LASVM and BMD_DXA increases the correlation with the *FL* to r=0.80. This indicates that these two quantities are complementary and explain better the biomechanical strength of femur specimens. In contrast, a multiregression model combining the α-fraction and BMD_QCT does not explain better the biomechanical strength. BMD_DXA is a global measure of mineralization that contains a contribution of the cortical bone. However, BMD_QCT was evaluated in the VOI's, thus no contribution of the cortical shell was considered. This fact may explain the different performances of these two quantities when combined with bone structure measures in multiregression models.

A comparison between results obtained using scaling indices and scaling vectors indicates that structure measures that account for the anisotropic nature of the trabecular structure are best suited to describe the biomechanical properties of human femur in vitro.

4. Conclusions

We have introduced a new anisotropic methodology, the so-called Locally Adapted Scaling Vector Method, to characterize structures in HRCT images of human bone tissue. The LASVM is able to account for the intrinsic orientation of the trabecular net of the proximal femur. This study showed that a more accurate bone structure characterization is achieved when a detailed assessment of local orientations is performed. Because of this fact, results obtained using the new 3D non-linear local texture measure are superior to those obtained using a 3D non-linear local isotropic texture measure and comparable to those given by BMD. This suggests that anisotropic texture measures have a superior performance than isotropic ones in cases where the image structure orientation plays a relevant role. We also found that models combining bone structure measures with BMD can better predict the mechanical properties of femoral specimens. This finding is in agreement with other studies (Link et al., 2003; Monetti et al. 2004; Wigderowitz et al., 2000) where it is suggested that structure characterization and BMD measurements should regularly be applied since they are complementary techniques and provide a great deal of information on the biomechanical properties of bone specimens.

5. Acknowledgments

This study was supported by the Deutsche Forschungsgemainschaft (DFG) under the grant MU 2288/2-2. The authors are very thankful to Ernst Rummeny for stimulating discussions. We also thank Simone Kohlmann, Volker Kuhn, and Maiko Matsuura for performing the biomechanical tests, and Holger Böhm, Simone Kohlmann, and Cecilia Wunderer for scanning the specimens.

6. References

Bauer, JS.; Kohlmann, S.; Eckstein, F.; Müller, D.; Lochmüller, EM. & Link, TM. (2006). Structural analysis of trabecular bone of the proximal femur using multislice

computed tomography: a comparison with dual X-ray absorptiometry for predicting biomechanical strength in vitro. *Calcif. Tissue Int.*, Vol. 78, No 2, pp.78–89

Baum, T.; Carballido-Gamio, J.; Huber, M.; Müller, D.; Monetti, R.; Räth, C.; Eckstein, F.; Lochmüller EM.; Majumdar, S.; Rummeny, E.; Link, T. & Bauer, JS. (2010). Automated 3D trabecular bone structure analysis of the proximal femur—prediction of biomechanical strength by CT and DXA. *Osteoporos. Int.*, Vol. 21, pp.1553-1564

Böhm, H.; Räth, C.; Monetti, R.; Müller, D.; Newitt, D.; Majumdar, S.; Rummeny, E.; Morfill, G. & Link, T. (2003). Local 3D Scaling Properties for the Analysis of Trabecular Bone extracted from High Resolution Magnetic Resonance Imaging of Human Trabecular Bone. *Investigative Radiology*, Vol. 38, pp.269-280

Boutry, N.; Cortet, B.; Dubois, P.; Marchandise, X. & Cotton, A. (2003). Trabecular bone structure of the calcaneous: preliminary in vivo MR imaging assessment in men with osteoporosis. *Radiology*, Vol. 227, pp. 708-717

Carballido-Gamio, J. & Majumdar S. (2006). Clinical utility of micro-architectural measurements of trabecular bone. *Curr. Osteoporos. Rep.*, Vol. 4, pp. 64-70

Center, J.R.; Nguyen, T.V.; Schneider, D.; Sambrook, P. & Eisman, J. (1999). Mortality after all major types of osteoporotic fracture in men and women: an observational study. *Lancet*, Vol. 353(9156), pp. 878-882

Ding, M. & Hvid, I. (2000). Quantification of age-related changes in the structure mdoel type and trabecular thickness of human tibial cancellous bone. *Bone,* Vol.26, No. 3, pp. 291-295

Eckstein, F.; Wunderer, C.; Böhm, H.; Kuhn, V.; Priemel, M.; Link, TM. & Lochmüller, EM. (2004). Reproducibility and side differences of mechanical tests for determining the structural strength of the proximal femur. *J. Bone Miner. Res.* Vol. 19, No 3, pp. 379–385

Grassberger, P.; Badii, R. & Politi, A. (1988). Scaling laws for invariant measures on hyperbolic and nonhyberbolic atractors. *Journal of Statistical Physics,* Vol. 51, No. 1/2, pp. 135-178

Gomberg, B.R.; Saha, P.K.; Song, H.K.; Hwang, S.N. & Wehrli, F. (2000). Application of topological analysis to magnetic resonance images of human trabecular bone. *IEEE Trans. Med. Imaging*, Vol. 19, pp. 166-174

Halsley, T.; Jensen, M.; et al. (1986). Fractal measures and their singularities: the characterization of strange sets. *Phys. Rev. A*, Vol. 33, pp.1141-1151

Hildebrand, T. & Rüegsegger, P. (1997a). A new method for the model-independent assessment of thickness in three-dimensional images. *J Microsc,* Vol. 185, Pt 1, pp. 67-75

Hildebrand, T. & Rüegsegger, P. (1997b). Quantification of bone microarchitecture with the Structure Model Index. *CMBBE,* Vol.1, pp.15-23

Hildebrand, T.;Laib, A.; Müller, R.; Dequeker, J. & Rüegsegger, P. (1999). Direct three-dimensional morphometric analysis of human cancellous bone: microstructural data from spine, femur iliac crest, and calcaneus. *J Bone Miner Res,* Vol. 14, No. 7, pp. 1167-1174

Huber, M.; Carballido-Gamio, J.; Bauer, JS; Baum, T.; Eckstein, F.; Lochmüller, EM; Majumdar, S. & Link, TM. (2008). Proximal femur specimens: automated 3D trabecular bone mineral density analysis at multidetector CT-correlation with biomechanical strength measurement. *Radiology*, Vol. 247, No. 2, pp. 472-481

Huiskes, R.; Ruimerman, R.; van Lenthe, G. & Janssen, J. (2000). Effects of mechanical forces on maintenance, adaptation of form in trabecular bone. *Nature*, Vol. 405, pp. 704-706

Jamitzky, F.; Stark, RW; Bunk, W.; Thalhammer, S.; Rath, C.; Aschenbrenner, T.; Morfill, G. & Heckel, W. (2000) Scaling-index method as an image processing tool in scanning-probe microscopy. *Ultramicroscopy*, Vol. 86, pp.241-246

Kanis, J.A. (2002). Diagnosis of osteoporosis and assessment of fracture risk. *Lancet*, Vol. 359, pp. 1929-1936

Kanis, J.A., on behalf of the World Health Organisation Scientific Group (2007). Assessment of osteoporosis at the primary health care level. *WHO Collaborating Centre for Metabolic Bone Diseases*, University of Sheffield

Krug, R.; Banerjee, S.; Han, E.; Newitt, D.; Link, T. & Majumdar, S. (2005). Feasibility of in vivo structural analysis of high-resolution magnetic resonance images of the proximal femur. *Osteoporos. Int.*, Vol. 16, pp. 1307-1314

Prevention and Management of Osteoporosis. (2003). *World Health OrganizationTechnical Report Series*, Vol. 921, pp. 1-164

Laib, A.; Newitt, D.; Lu, Y. & Majumdar, S. (2002). New model independent measures of trabecular bone structure applied to in vivo high-resolution MR images. *Osteoporos. Int.*, Vol. 13, pp. 130-136

Link, T.; Majumdar, S.; Grampp, S.; Gugliemi, G.; van Kuijk, C.; Imhof, H.; Glueer, C. & Adams, J. (1998). A comparative study of trabecular bone properties in the spine and femur using high resolution MRI and CT," *J. Bone Miner. Res.*, Vol. 13, pp. 122-132

Link, T.; Majumdar, S.; Lin, J.; Newitt, D.; Augat, P.; Ouyang, X.; Mathur, A. & Genant, H. (1999). Imaging of trabecular bone structure in osteoporosis. *Europ. Radiol.*, Vol. 9, pp. 1781-1788

Link, T.; Vieth, V.; Matheis, J.; Newitt, D.; Lu, Y.; Rummeny, E. & Maj, S. (2002). Bone structure of the distal radius and the calcaneous versus BMD of the spine and proximal femur in the prediction of osteoporotic spine fractures. *Eur. Radiol.*, Vol. 12, pp. 401-408

Majumdar, S.; Newitt, D.; Mathur, A.; Osman, D.; Gies, A.; Chiu, E.; Lotz, J.; Kinney, J. & Genant, H. (1996). Magnetic resonance imaging of trabecular bone structure in the distal radius: relationship with X-Ray tomographic microscopy and biomechanics. *Osteoporos. Int.*, Vol. 6, pp. 376-385

Majumdar, S.; Link, T.; Augat, P.; Lin, J.; Newitt, D.; Lane, N. & Genant, H. (1999). Trabecular bone architecture in the distal radius using MR imaging in subjects with fractures of the proximal femur. *Osteoporos. Int.*, Vol. 10, pp. 231-239

Monetti, R.A.; Böhm, H.; Müller, D.; Newitt, D.; Majumdar, S.; Rummeny, E.; Link, T.M. & Räth, C. (2003). Scaling Index Method: a novel nonlinear technique for the analysis

of high-resolution MRI of human bones. *Proceedings of Medical Imaging Conference of SPIE,* Vol. 5032, pp. 1777-1786

Monetti, R.A.; Böhm, H.; Müller, D.; Rummeny, E.; Link, T. & Räth, C. (2004). Assessing the biomechanical strength of trabecular bone in vitro using 3D anisotropic non- linear texture measures: The Scaling Vector Method. *Proceedings of Medical Imaging Conference of SPIE,* Vol. 5370, pp. 215-224

Monetti, R.A.; Bauer, J.; Müller, D.; Rummeny, E.; Matsuura, M.; Eckstein, F.; Link, T. & Raeth, C. (2007). Application of the Scaling Index Method to μ-CT images of human trabecular bone for the characterization of biomechanical strength. *Proceedings of Medical Imaging Conference of SPIE,* Vol. 6512, pp. 65124H

Monetti, R.A.; Bauer, J.; Sidorenko, I.; Müller, D.; Rummeny, E.; Matsuura, M.; Eckstein, F.; Lochmüller, E.M.; Zysset, P. & Räth, C. (2009). Assessment of the human trabecular bone structure using Minkowski Functionals. *Proceedings of Medical Imaging Conference of SPIE,* Vol. 7262, pp. 72620N

Müller, D.; Link, T.M.; Monetti, R.; Bauer, J.; Böhm, H.; Seifert-Klauss, V.; Rummeny, E.J.; Morfill, G.E. & Räth, C. (2006). The 3D-based scaling index algorithm: a new structure measure to analyze trabecular bone architecture in hifh-resolution MR images in vivo. *Osteoporos. Int.,* Vol. 17, pp. 1783-1493

Osteoporosis: Clinical Guidelines for Prevention and Treatment. (1999). *Royal College of Physicians*. Lavenham Press, Sudbury, Suffolk

Parfitt, M.; Drezner, M.; et al. (1987). Bone Histomorphometry: Standardization of nomenclature, symbols and units. Report of the ASBMR histomorphometry nomenclature committee. *J. Bone Miner. Res.*, Vol. 2, pp.595-610

Paladini, G. & Vulpiani, A. (1987). Anomalous scaling laws in multiftactal objects. *Phys Reports,* Vol. 156, No. 4, pp. 147-225

Phan, C.M.; Matsuura, M.; Bauer, J.; Dunn, T.; Newitt, D.; Lochmueller, E.; Eckstein, F.; Majumdar, S. & Link, T. (2006). Trabecular bone structure of the calcaneous: comparison of MR imaging at 3.0 and 1.5 T with micro-CT as the standard of reference. *Radiology*, Vol. 239, pp. 488-496

Räth, C. & Morfill, G. (1997). Texture detection and texture duscrimination with anisotropic scaling indices. *J. Opt. Soc. Am. A,* Vol. 14, No. 12, pp. 3208-3215

Räth, C.; Bunk, W.; Huber, M.B.; Morfill, G.E.; Retzlaff, J. & Schücker, P. (2002). Analysing large-scale structure –I. Weighted scaling indices and constrained randomization. *Mon. Not. R. Astron. Soc.,* Vol. 337, pp. 413-421

Räth, C.; Monetti, R.; Böhm, H.; Müller, D.; Rummeny, E. & Link, T. (2003). Analysing and selecting measures for quantifying trabecular bone structures using surrogates. *Proceedings of Medical Imaging Conference of SPIE,* Vol. 5032, pp. 1748-1756

Räth, C. & Schücker, P. (2003). Analysing large scale structure - II. Testing for primordial non-Gaussianity in CMB maps using surrogates. *Mon. Not. R. Astron. Soc*, Vol. 344, pp.115-128

Räth, C.; Monetti, R.; Bauer, J.; Sidorenko, I.; Müller, D.; Matsuura, M.; Lochmüller, E.-M.; Zysset, P. & Eckstein, F. (2008). Strength through structure: visualization and local assessment of the trabecular bone structure. *New Journal of Physics,* Vol. 10, pp. 125010-125027

Saha, P. & Wehrli F. (2004). A robust method for measuring trabecular bone orientation anisotropy at in vivo resolution using tensor scale. *Patt. Recog*., Vol. 37, pp. 1935-1944

Vieth, V.; Link, T.; et al. (2001). Does the trabecular structure depicted by high-resolution MRI of the calcaneous reflect the true bone structure? *Invest. Radiol*., Vol. 36, pp. 210-217

Wehrli, F.W. (2007). Structural and functional assessment of trabecular and cortical bone by micro-magnetic resonance imaging. *J. Magn. Reson. Imaging*, Vol. 25, pp. 390-409

Wigderowitz, C.A.; Paterson, C.R.; Dashti, H.; McGurty, D. & Rowley, D. (2000). Prediction of bone strength from Cancellous structure of the distal radius: Can we improve on DXA? *Osteoporos. Int*., Vol. 11, pp. 840-846

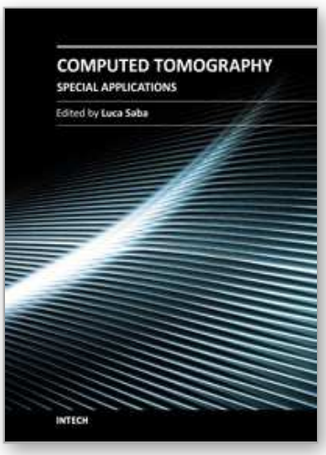

Computed Tomography - Special Applications
Edited by Dr. Luca Saba

ISBN 978-953-307-723-9
Hard cover, 318 pages
Publisher InTech
Published online 21, November, 2011
Published in print edition November, 2011

CT has evolved into an indispensable imaging method in clinical routine. The first generation of CT scanners developed in the 1970s and numerous innovations have improved the utility and application field of the CT, such as the introduction of helical systems that allowed the development of the "volumetric CT" concept. Recently interesting technical, anthropomorphic, forensic and archeological as well as paleontological applications of computed tomography have been developed. These applications further strengthen the method as a generic diagnostic tool for non destructive material testing and three dimensional visualization beyond its medical use.

InTech Europe
University Campus STeP Ri
Slavka Krautzeka 83/A
51000 Rijeka, Croatia
Phone: +385 (51) 770 447
Fax: +385 (51) 686 166
www.intechopen.com

InTech China
Unit 405, Office Block, Hotel Equatorial Shanghai
No.65, Yan An Road (West), Shanghai, 200040, China
中国上海市延安西路65号上海国际贵都大饭店办公楼405单元
Phone: +86-21-62489820
Fax: +86-21-62489821

IntechOpen